HHS Public Access

Author manuscript

J Vis Exp. Author manuscript; available in PMC 2022 January 01.

Convection Enhanced Delivery (CED) of Optogenetic Adeno-associated viral (AVV) vector to the Cortex of Rhesus Macaques under guidance of online MRI images

Karam Khateeb[1,2], **Devon J. Griggs**[2,3], **Philip N. Sabes**[4], **Azadeh Yazdan-Shamorad**[1,2,3,4,5]

[1]Department of Bioengineering, University of Washington, Seattle, WA, USA

[2]Washington National Primate Research Center, Seattle, WA, USA

[3]Department of Electrical and Computer Engineering, University of Washington, Seattle, WA, USA

[4]Department of Physiology and Center for Integrative Neuroscience, University of California San Francisco, San Francisco, CA, USA

LONG ABSTRACT:

In non-human primate (NHP) optogenetics, infecting large cortical areas with viral vectors is often a difficult and time-consuming task. Here we demonstrate the use of magnetic resonance (MR)-guided convection enhanced delivery (CED) of optogenetic viral vectors into primary somatosensory (S1) and motor (M1) cortices of macaques to obtain efficient, widespread cortical expression of light-sensitive ion channels. Adeno-associated viral (AAV) vectors encoding the red-shifted opsin C1V1 fused to yellow fluorescent protein (EYFP) were injected into the cortex of rhesus macaques under MR-guided CED. Three months post-infusion, epifluorescent imaging confirmed large regions of optogenetic expression (>130 mm^2) in M1 and S1 in two macaques. Furthermore, we were able to record reliable light-evoked electrophysiology responses from the expressing areas using micro-electrocorticographic arrays. Later histological analysis and immunostaining against the reporter revealed widespread and dense optogenetic expression in M1 and S1 corresponding to the distribution indicated by epifluorescent imaging. This technique enables us to obtain expression across large areas of cortex within a shorter period of time with minimal damage compared to the traditional techniques and can be an optimal approach for optogenetic viral delivery in large animals such as NHPs. This approach demonstrates great potential for network-level manipulation of neural circuits with cell-type specificity in animal models evolutionarily close to humans.

SHORT ABSTRACT:

Here we demonstrate magnetic resonance (MR)-guided convection enhanced delivery (CED) of viral vectors into the cortex as an efficient and simplified approach for achieving optogenetic expression across large cortical areas in the macaque brain.

[5]*Corresponding Author:* Azadeh Yazdan-Shahmorad, azadehy@uw.edu, Tel: (206)-543-6127.

DISCLOSURES:
PNS has financial interest in Neuralink Corp., a company that is developing clinical therapies using brain stimulation.

Keywords

Optogenetics; Non-human primates; Rhesus Macaques; Viral vector delivery; Opsin expression; Primary motor cortex; Primary somatosensory cortex

INTRODUCTION:

Optogenetics is a powerful tool that allows for the manipulation of neural activity and the study of network connections in the brain. Implementing this technique in non-human primates (NHPs) has the potential to enhance our understanding of large-scale neural computation, cognition, and behavior in the primate brain. Although optogenetics has been successfully implemented in NHPs in recent years[1–7], a challenge that researchers face is achieving high levels of expression across large brain areas in these animals. Here, we are providing an efficient and simplified approach to achieve high levels of optogenetic expression across large areas of cortex in macaques. This technique has great potential to improve current optogenetic studies in these animals in combination with state-of-the-art recording[8,9] and optical stimulation[10] technologies.

Convection enhanced delivery (CED) is an established method of delivery of pharmacological agents and other large molecules, including viral vectors, to the central nervous system[11–13]. Whereas conventional delivery methods involve multiple low volume infusions distributed across small regions of the brain, CED can achieve broader and more even agent distribution with fewer infusions. Pressure-driven bulk fluid flow (convection) during infusion allows for more widely and uniformly distributed transduction of the target tissue when delivering viral vectors with CED. In recent studies, we demonstrated the transduction and subsequent optogenetic expression of large areas of primary motor (M1) and somatosensory (S1) cortices[9] and thalamus[14] using magnetic resonance (MR)-guided CED.

Here we outline the use of CED to achieve optogenetic expression across large cortical areas with only a few cortical injections.

PROTOCOL:

All procedures have been approved by the University of California, San Francisco Institutional Animal Care and Use Committee (IACUC) and are compliant with the Guide for the Care and Use of Laboratory Animals. The following procedure was performed using two adult male rhesus macaques of 8 and 7 years of age, weighing 17.5 kg and 16.5 kg (monkey G and monkey J), respectively.

Use standard aseptic techniques for all surgical procedures.

1. Baseline Imaging

1.1 Sedate and intubate the animal and maintain general anesthesia under isoflurane (concentration changed between 0 to 5% as needed). Monitor the animal’s temperature,

heart rate, oxygen saturation, electrocardiographic responses, and end-tidal partial pressure of CO_2 throughout the procedure.

1.2 Place the animal in an MR-compatible stereotaxic frame (see the Table of Materials) in which it will remain throughout the procedure. Connect the animal to a portable MR-compatible isoflurane machine and transport it to the MRI scanner.

1.3 Acquire standard T1 (flip angle = 9°, repetition time/echo time = 668.6, matrix size = 192 × 192 × 80, slice thickness = 1 mm) and T2 (flip angle = 130°, repetition time/echo time = 52.5, matrix size = 256 × 256 × 45, slice thickness = 1 mm) anatomical MR images as baseline reference and for surgical planning.

1.4 Recover the animal from anesthesia and transport it to the animal housing area.

1.5 Use the acquired T1 and T2 images to determine the placement of the craniotomy. The location of the craniotomy can be precisely determined by matching the cortical area of the interest from MR with the macaque brain atlas. In addition, these baseline images can provide an estimate for the locations of viral infusion.

2. MR-Compatible Chamber Implantation

2.1 Sedate and intubate the animal and maintain general anesthesia with standard anesthetic monitoring as in 1.1.

2.2 Place the animal in the MR-compatible stereotaxic frame in which it will remain throughout chamber implantation and viral vector delivery. Connect the animal to a portable MR-compatible isoflurane machine.

2.3 Create a sagittal incision approximately 2 cm from the midline with a length of about 5 cm with a scalpel.

2.4 Remove the underlying soft tissue from the skull using elevators (see Table of Materials).

2.5 Create a circular craniotomy (2.5 cm diameter) to cover the pre-planned trajectories for injections using a trephine (see Table of Materials).

2.5.1 Lower the centering point of the trephine past the edge of the trephine. Create an indentation at the center of the planned craniotomy sufficiently deep in the skull to anchor the trephine using the adjustable centering point of the trephine. Exercise caution to avoid completely penetrating through the depth of the skull as this could cause damage to the underlying neural tissue.

2.5.2 Periodically flush the area with saline as needed to maintain tissue moisture throughout the craniotomy.

2.5.3 Once the center has been made, lower the trephine onto the skull and rotate the trephine clockwise and counterclockwise while applying downward pressure until the bone

cap can be removed with forceps. Exercise caution to avoid damaging the underlying tissue with the trephine.

2.6 Thread a fine suture (size 6–0) to the dura in the center of the craniotomy and lift the dura by gentling pulling the thread from the surface of the brain creating a tent in the center of the craniotomy.

2.7 Next, puncture the dura close to the center of the tent using fine ophthalmic scissors to avoid damaging the brain. Then cut the dura from the center to the edge of the craniotomy and continue along the edge with fine opthalmic scissors.

2.8 Mount the cylindrical custom-made CED MR-compatible chamber (Figure 1; see section 4 for production instructions) to the skull on top of the craniotomy to provide cannula support during CED infusion such that the curvature of the chamber flange aligns well with the curvature of the skull.

2.9 Secure the implants to the skull using either plastic screws and dental acrylic or a few titanium screws.

3. Viral Vector Delivery

3.1 Soon after implanting the MR-compatible chamber and inserting the cannula injection grid (Figure 1A-B, Supplementary Figure 1) into the chamber, fill the grid with saline for visualizing the injection locations via MR anatomical images and fill the chamber cavities with wet gelfoam to maintain moisture of the brain (Figure 1F).

3.2 Cover the skin and the cylinder with a sterile antimicrobial incise drape to maintain the sterility of the cylinders during transport and MR infusions. Place a vitamin E capsule to mark the top of the injection grid for positive identification.

3.3 While the animal remains intubated, detach the endotracheal tube from the anesthesia circuit and reattach it to a portable MR-compatible isoflurane machine and transport the animal to the MRI scanner.

3.4 Acquire T1 (flip angle = 9°, repetition time/echo time = 668.6, matrix size = 192 × 192, slice thickness= 1 mm, 80 slices) images to calculate the distance from the top of the injection grid and the cortical surface. The vitamin E capsule is clearly visible in T1 images and should be used as a marker for the top of the injection grid (Figure 2A). The MR imaging software, provides a ruler which enables measuring distance in metrics from different planes.

3.5 Acquire T2 (flip angle = 130°, repetition time/echo time = 52.5, matrix size = 256 × 256, slice thickness = 1 mm, 45 slices) images to determine the optimal cannula guides for each site based on the targeted site of infusion (Figure 2B-C). As mentioned earlier, the cannula grid is filled with saline which is best visible in T2 images. Using the MR imaging software, scroll through the coronal and sagittal planes to find the ideal location of infusion.

3.6 After thawing the viral vector for a few hours at room temperature, mix the viral vector with the MR contrast agent Gadoteridol (Ratio of 250:1; 2mM Gd-DTPA, see Table of Materials) by pipette or vortex mixing. The presented technique was tested for AAV vectors with a CamKIIa promoter driving expression of C1V1 fused to EYFP (AAV2.5-CamKII-C1V1-EYFP, titer: 2.5×10^{12} virus molecules/ml; see Table of Materials).

3.7 Load the mixed virus into a 0.2 mL high pressure IV tubing (see Table of Materials).

3.8 Establish a sterile field outside the MR scanner for preparing the viral infusion line.

3.9 Using high pressure IV tubing, connect a long extension line (approximately 3–5 meters, depending on the location of the infusion pump with respect to the MR bore) to an MR-compatible 3 cc syringe and prime with saline.

3.10 Connect the syringe to 0.2 mL IV tubing loaded with the virus and attach the reflux-resistant cannula with a 1 mm stepped tip (Figure 2D; see section 5 for cannula production instructions) to the distal end of this assembly with a perifix clamp style catheter connector (see table of materials) (Figure 2E).

3.11 Lastly, set the syringe in an MR-compatible pump (see table of materials). Place the pump controller in the scanner control room as it is not MR-compatible.

3.12 Using the baseline anatomical MR images obtained before, select the cannula injection grid location and insertion depth needed to reach the target infusion site. Mark the insertion depth on the cannula using sterile tape.

3.13 Begin the infusion at a rate of 1 μl/min and visually validate the flow of the fluid in the infusion line by observing the ejection of fluid from the cannula tip.

3.14 Insert the cannula manually through the injection grid to the target depth while maintaining flow in the infusion line, as this will prevent the penetrated tissue from clogging the cannula during insertion.

3.15 Acquire fast (2 minute) flash T1 weighted images (flip angle = 30°, repetition time/ echo time = 3.05, matrix size = 128 × 128, slice thickness = 1 mm, 64 slices) for online monitoring of the viral vector infusion.

3.16 After infusing ~10 μL of the vector such that enough virus is infused to detect in the MR scanner, obtain MR images to verify correct cannula placement. If the depth of the inserted cannula is incorrect, adjust the depth accordingly or slowly remove the cannula and re-attempt the insertion as in 3.12.

3.17 Monitor the infusion via guidance of online MR images (flash T1 weighted) and increase the infusion rate to 5 μL/min by 1 μL/min steps every few minutes (Figure 3A).

3.18 After infusing approximately 40 μL of the viral vector, begin reducing the infusion rate by 1 μL/min steps and stop the infusion after ~50 μL is injected and leave the cannula in place for 10 minutes.

3.19 Slowly remove the cannula from the brain and move to the next location. Repeat steps 3.8 to 3.15 for each location.

3.20 Cover the cylinder with a sterile drape at the end of injections, before animal transport. Then transport the animal back to the operating room.

3.21 Either explant the MR-compatible chamber and close the surgical incision by replacing the bone flap and overlying muscle and suturing the skin using standard aseptic techniques or replace the chamber with a titanium cylinder and artificial dura (see Yazdan-Shahmorad *et al.* 2016[9]) for neural recording and stimulation.

4. MR-Compatible Chamber Production

4.1 Fabricate the nylon cannula injection grid (Figure 1A-B) by machining according to the specified dimensions (Supplementary Figure 1).

4.2 3D print the MR-compatible cylinder out of acrylonitrile butadiene styrene (ABS0 plastic; Figure 1C-E; see Supplementary File 1-3; see Table of Materials for 3D printer and materials). One design maintains a fixed cannula injection grid within the MR-compatible cylinder (Figure 1C), while another allows for rotation of the grid, extending the injection region (Figure 1D-E).

NOTE: One design maintains a fixed cannula injection grid within the MR-compatible cylinder (Figure 1C), while another allows for rotation of the grid, extending the injection region (Figure 1D-E).

4.3 Thread the cannula injection grid and tap the corresponding cavity of the MR-compatible chamber such that both pieces exhibit the same threading. Any type of threading can be used provided that both components have the same threading.

NOTE: Any type of threading can be used provided that both components have the same threading.

4.4 Insert the nylon cannula injection grid by screwing into the tapped hole of the MR-compatible cylinder.

5. Reflux-resistant Cannula Production

5.1 Cut a 30 cm silica tubing with 0.32 mm ID and 0.43 mm OD for the inner silica tubing (see table of materials) using a razor blade.

5.2 Cut a 7.5 cm and a 5 cm silica tubing with 0.45 mm ID and 0.76 mm OD for the outer silica tubing (see table of materials).

5.3 Adhere the 7.5 cm outer tubing to the 30 cm inner tubing with cyanoacrylate such that the inner tube extends 1 mm beyond the outer tube, making the reflux-resistant step (Figure 2D). To ensure that the cyanoacrylate does not enter the inside of the inner tubing, place the cyanoacrylate on the outside of the inner tubing far from the cannula tip.

5.4 Paste the 5 cm silica tubing to the other end of the inner tubing for attachment to the perifix clamp style catheter connector (see step 3.10).

REPRESENTATIVE RESULTS:

Convection Enhanced Delivery (CED) under MRI Guidance

The spread of the viral vector was monitored during CED infusion under the guidance of online MR images (Figure 3A). In this study, S1 and M1 of two monkeys were targeted (Figure 3B). The three-dimensional distribution volumes were estimated in a post-hoc analysis of the MR images (Figure 3C) as described by Yazdan-Shahmorad *et al.* 2016[9], confirming coverage of large areas of cortex. The M1 infusions for monkey G were done without MR guidance due to time constraints.

Validation of Viral Expression

Large cortical optogenetic expression was confirmed by epifluorescent imaging, electrophysiological recordings, and histological analysis as described by Yazdan-Shahmorad *et al.* 2016[9]. We monitored optogenetic expression by surface epifluorescence imaging of the fluorescent reporter [2,9] and estimated more than 130 mm^2 of expression along the cortical surface in M1 and S1 of two macaques from only three cortical injections[9,15]. Light stimulation (488 nm, 20 mW power at the tip; see table of materials) yielded reliable electrophysiological responses in the expressing areas as measured by semi-transparent micro-electrocorticographic arrays[8,9,16] (Figure 4).

Analysis of the MR images yielded an estimated 233 mm^3 and 433 mm^3 of vector spread in M1 and S1 of monkey J, respectively, and 317 mm^3 in S1 of monkey G[9]. We performed histological analyses on serial coronal sections and observed large-scale optogenetic expression around the infusion sites in M1 and S1 (Figure 5A-B), with an estimated 70–80% of cells expressing the opsin. The expression observed from histology aligned with the estimated expression distribution from epifluorescent imaging (Figure 5A-D). One of the two infusions performed outside of the MR scanner in monkey G was unsuccessful, yielding no expression in the corresponding region (Figure 5D). The spread estimated from MR imaging was completely within the bounds of both the epifluorescent and the histological measures of viral spread (Figure 5E-G). The expansion of the epifluorescent imaging beyond the MR estimate can be attributed to the diffusion of viral particles beyond the advection region. Moreover, the histological estimate extended beyond the epifluorescence estimate due to a lack of optical access beyond the craniotomy. The details of these techniques are included in our previous paper[9].

DISCUSSION:

Here we outline a feasible and efficient technique for achieving large-scale optogenetic expression in NHP primary somatosensory and motor cortex by MR-guided CED. The use of MR-guided CED presents significant advantages over traditional methods of viral infusion in the NHP brain. One such advantage is the ability to attain expression over large areas with fewer required infusions. For instance, with conventional methods, multiple injections of 1–2 μL of the vector yield expression in a 2–3 mm diameter region[1,2,5,17].

While previous attempts at achieving large-scale vector spread have yielded expression volumes of approximately 10 mm^3 with multiple injections[18], here we present a method to achieve expression over 200 mm^3 with only a few infusions. A single infusion of 50 μL by CED can achieve vector spread up to 10 mm from the injection site for cortical CED[9] and full coverage of frontal cortical areas with thalamic CED[14]. Furthermore, it has been shown that using CED can achieve more homogeneous distribution of the injected agent[12,19–22], leading to uniform expression levels around the site of viral vector infusion, compared to traditional microinjections. In our experiments employing CED, we observed uniformly high expression levels with approximately 70–80% of neurons expressing the opsin[8,9] (Figure 4). In contrast, conventional diffusion-based injections exhibit regions of high expression concentrated near injection sites enveloped by weakening expression levels[4,5,17]. The reduced need for multiple injections renders CED infusion a time-efficient method of obtaining large-scale, uniform optogenetic expression. Due to the smaller number of injections and faster infusion rates, we were able to plan and infuse the viral vector under the guidance of MRI. The use of online MR images enables precise targeting of infusions and the monitoring of the spread of the viral vector during infusion. However, if the initial depth of the inserted cannula is incorrect, this may yield expression in undesired locations as a result of the initial infused ~10 μL needed to visually detect the infusion via MR. Alternatively, commercial neurosurgical navigation systems utilizing fiducial markers can also be employed in place of MR guidance. Additionally, the costs of online imaging may be circumvented by marking the desired depth of insertion on the cannula prior to insertion and visual confirmation of complete infusion, although the accuracy of the cannula placement would be reduced. However, as seen by the unsuccessful injection in M1 of monkey G (Figure 5D), MR guidance can be critical for ensuring successful infusion.

Previous studies have demonstrated the safety of CED infusions of both non-viral and viral particles with no observed tissue damage outside the cannula tract and no behavioral deficits[9,11–15,20]. Here and in our previous publications[9,14] we report similar results following CED infusion of optogenetic viral vectors. In addition to no observed behavioral deficits following infusion, NeuN and Nissl[9,14,15] staining revealed neuronal cell death and gliosis was limited only to the cannula tract, as has been reported with diffusion-based methods[5]. To minimize the damage from the cannula track, we can potentially reduce the diameter of the cannula. However, further investigation is needed to assess the effect of cannula size reduction on achieving large areas of expression. Moreover, because high infusion rates can also lead to tissue damage[13], it is recommended to maintain an infusion rate at or below 5 μL/min. For more detailed information about the CED technique please see our previous publication[9].

The use of MR-guided CED for attaining broad regions of targeted optogenetic expression in the primate cortex can lead to further investigations of large-scale circuit dynamics, neural plasticity, and network connectivity.

Supplementary Material

Refer to Web version on PubMed Central for supplementary material.

ACKNOWLEDGMENTS:

This work was supported by American Heart Association postdoctoral fellowship (AY), Defense Advanced Research Projects Agency (DARPA) Reorganization and Plasticity to Accelerate Injury Recovery (REPAIR; N66001-10-C-2010), R01.NS073940, and by the UCSF Neuroscience Imaging Center. We thank Camilo Diaz-Botia, Tim Hanson, Viktor Kharazia, Karen J. MacLeod, Juliana Milani, and Blakely Andrews for their help with the experiments and Nan Tian, Jiwei He, Peter Ledochowitsch and Michel Maharbiz for technical help.

REFERENCES:

1. Ruiz O et al. Optogenetics through windows on the brain in the nonhuman primate. J Neurophysiol. 110 (6), 1455–1467, (2013). [PubMed: 23761700]
2. Diester I et al. An optogenetic toolbox designed for primates. Nat Neurosci. 14 (3), 387–397, (2011). [PubMed: 21278729]
3. Ohayon S, Grimaldi P, Schweers N & Tsao DY Saccade modulation by optical and electrical stimulation in the macaque frontal eye field. J Neurosci. 33 (42), 16684–16697, (2013). [PubMed: 24133271]
4. Gerits A et al. Optogenetically induced behavioral and functional network changes in primates. Curr Biol. 22 (18), 1722–1726, (2012). [PubMed: 22840516]
5. Jazayeri M, Lindbloom-Brown Z & Horwitz GD Saccadic eye movements evoked by optogenetic activation of primate V1. Nat Neurosci. 15 (10), 1368–1370, (2012). [PubMed: 22941109]
6. Dai J, Brooks DI & Sheinberg DL Optogenetic and electrical microstimulation systematically bias visuospatial choice in primates. Curr Biol. 24 (1), 63–69, (2014). [PubMed: 24332543]
7. Afraz A, Boyden ES & DiCarlo JJ Optogenetic and pharmacological suppression of spatial clusters of face neurons reveal their causal role in face gender discrimination. Proc Natl Acad Sci U S A. 112 (21), 6730–6735, (2015). [PubMed: 25953336]
8. Ledochowitsch P et al. Strategies for optical control and simultaneous electrical readout of extended cortical circuits. J Neurosci Methods. 256 220–231, (2015). [PubMed: 26296286]
9. Yazdan-Shahmorad A et al. A Large-Scale Interface for Optogenetic Stimulation and Recording in Nonhuman Primates. Neuron. 89 (5), 927–939, (2016). [PubMed: 26875625]
10. Ju N, Jiang R, Macknik SL, Martinez-Conde S & Tang S Long-term all-optical interrogation of cortical neurons in awake-behaving nonhuman primates. PLoS Biol. 16 (8), e2005839, (2018). [PubMed: 30089111]
11. Bankiewicz KS et al. Convection-enhanced delivery of AAV vector in parkinsonian monkeys; in vivo detection of gene expression and restoration of dopaminergic function using pro-drug approach. Exp Neurol. 164 (1), 2–14, (2000). [PubMed: 10877910]
12. Kells AP et al. Efficient gene therapy-based method for the delivery of therapeutics to primate cortex. Proc Natl Acad Sci U S A. 106 (7), 2407–2411, (2009). [PubMed: 19193857]
13. Krauze MT et al. Reflux-free cannula for convection-enhanced high-speed delivery of therapeutic agents. J Neurosurg. 103 (5), 923–929, (2005). [PubMed: 16304999]
14. Yazdan-Shahmorad A et al. Widespread optogenetic expression in macaque cortex obtained with MR-guided, convection enhanced delivery (CED) of AAV vector to the thalamus. J Neurosci Methods. 293 347–358, (2018). [PubMed: 29042259]
15. Yazdan-Shahmorad A, Silversmith DB, Kharazia V & Sabes PN Targeted cortical reorganization using optogenetics in non-human primates. Elife. 7, (2018).
16. Yazdan-Shahmorad A et al. Demonstration of a setup for chronic optogenetic stimulation and recording across cortical areas in non-human primates. SPIE BiOS. (2015).
17. Lerchner W, Corgiat B, Der Minassian V, Saunders RC & Richmond BJ Injection parameters and virus dependent choice of promoters to improve neuron targeting in the nonhuman primate brain. Gene Ther. 21 (3), 233–241, (2014). [PubMed: 24401836]
18. Acker L, Pino EN, Boyden ES & Desimone R FEF inactivation with improved optogenetic methods. Proc Natl Acad Sci U S A. 113 (46), E7297–E7306, (2016). [PubMed: 27807140]
19. Bobo RH et al. Convection-enhanced delivery of macromolecules in the brain. Proc Natl Acad Sci U S A. 91 (6), 2076–2080, (1994). [PubMed: 8134351]

20. Lieberman DM, Laske DW, Morrison PF, Bankiewicz KS & Oldfield EH Convection-enhanced distribution of large molecules in gray matter during interstitial drug infusion. J Neurosurg. 82 (6), 1021–1029, (1995). [PubMed: 7539062]

21. Lonser RR, Gogate N, Morrison PF, Wood JD & Oldfield EH Direct convective delivery of macromolecules to the spinal cord. J Neurosurg. 89 (4), 616–622, (1998). [PubMed: 9761056]

22. Szerlip NJ et al. Real-time imaging of convection-enhanced delivery of viruses and virus-sized particles. J Neurosurg. 107 (3), 560–567, (2007). [PubMed: 17886556]

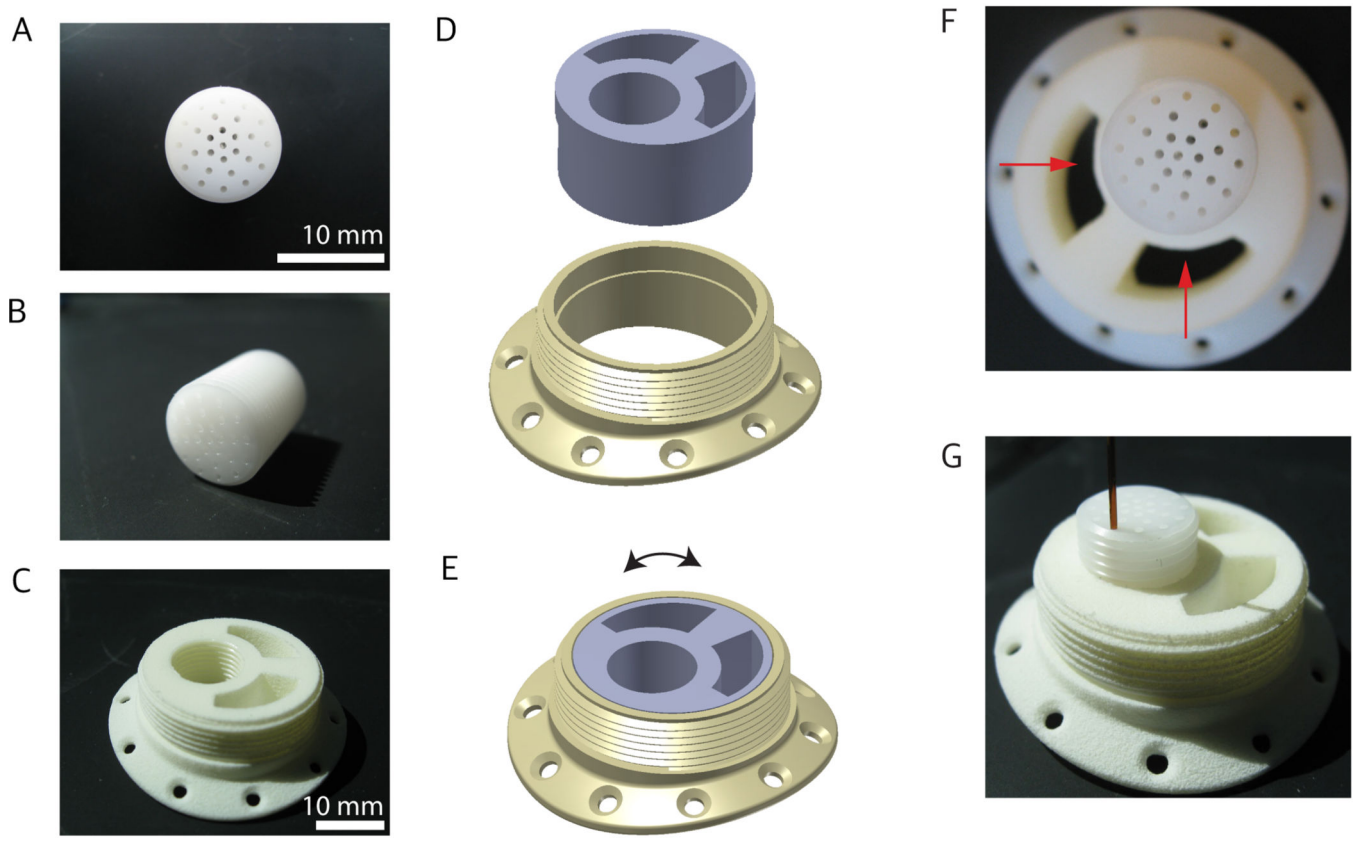

Figure 1.

MR-compatible cylinder and cannula injection grid. A,B) custom-designed nylon injection grid. C) MR-compatible fixed cylinder. D, E) Rotating MR-compatible cylinder. F) MR-compatible infusion cylinder with fixed grid position. The arrows point to the cavities that are designed to be filled with wet sterile absorbable gelatin keeping the surface of the brain moist for the duration of injection. G) Cannula inserted in the grid. This figure has been modified from Yazdan-Shahmorad *et al.* 2016[9].

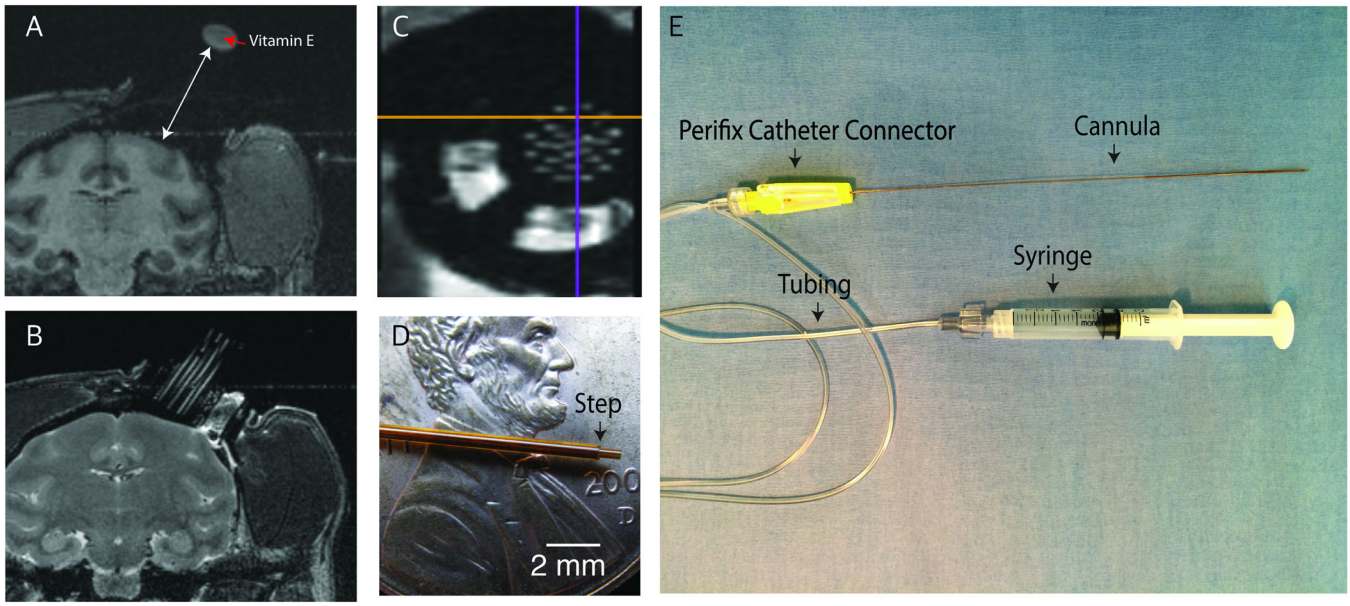

Figure 2.

A) T1-weighted image of vitamin E that was attached to the top of the injection grid that enables us to measure the distance to the surface of the brain (white arrow). B) T2-weighted image of the brain helps to plan the location of injection from the cannula grid filled with saline. C) MR image of the infusion chamber and the saline-filled cannula grid. The orthogonal lines represent the sagittal (yellow) and coronal (purple) planes. D) Photo of the reflux resistant injection cannula tip with the reflux resistant step (black arrow). E) Infusion lines. This figure has been modified from Yazdan-Shahmorad *et al.* 2016[9].

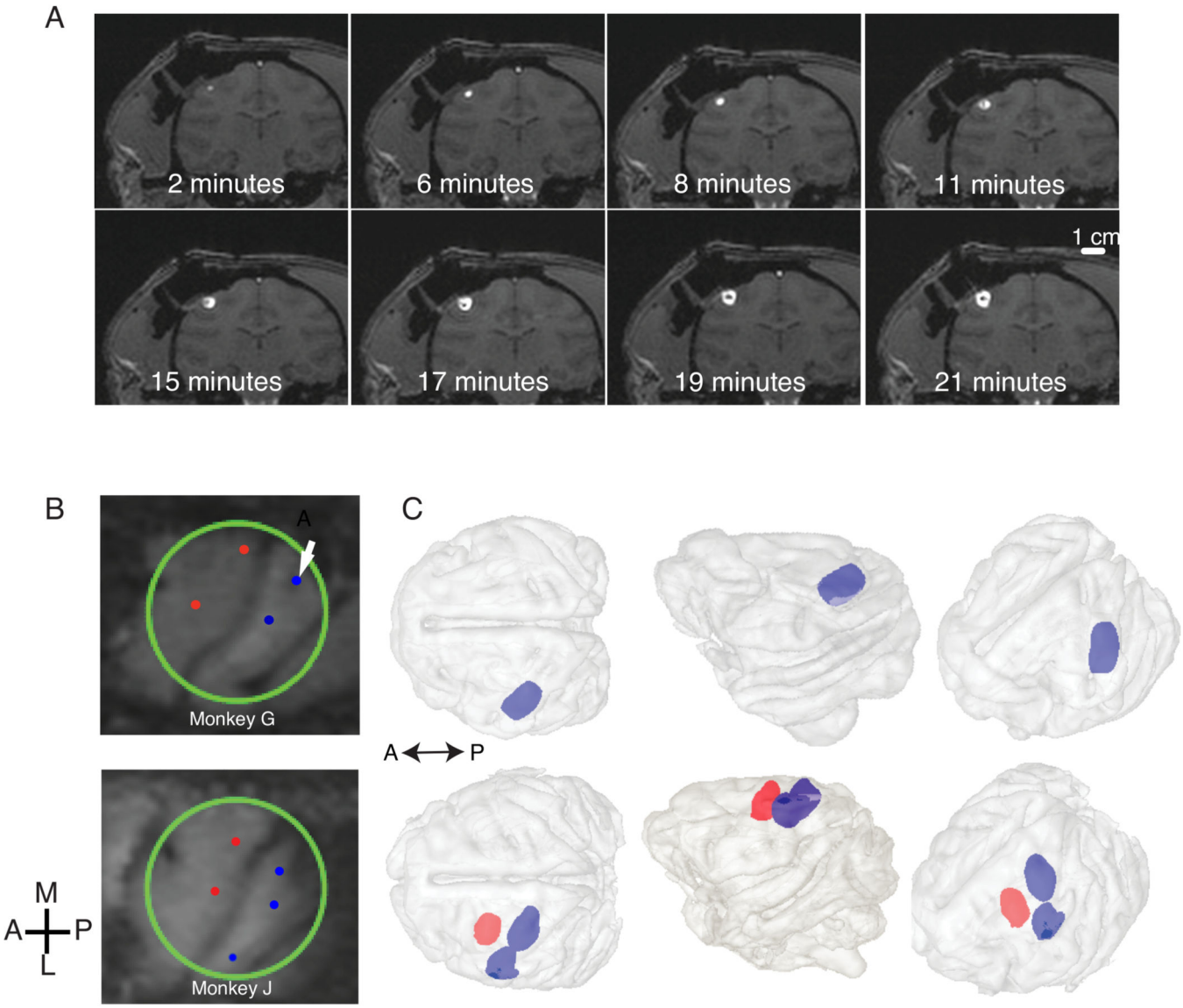

Figure 3.

A) Spread of 50 μL of the viral vector in coronal sections of Monkey G for one injection site in S1 (shown with an arrow in B). B) MRI surface rendering of the cortical surface below the cylinder for Monkeys G and J, respectively. The S1 infusion locations are shown in blue, M1 locations in red. C) MR Volume reconstruction of the spread of viral vector during CED infusion. Brain is shown in light gray; S1 and M1 infusion volumes are shown in blue and red, respectively. No MR volume reconstruction is available for the M1 infusions for monkey G since they were not done in the MR scanner. This figure has been modified from Yazdan-Shahmorad *et al.* 2016[9].

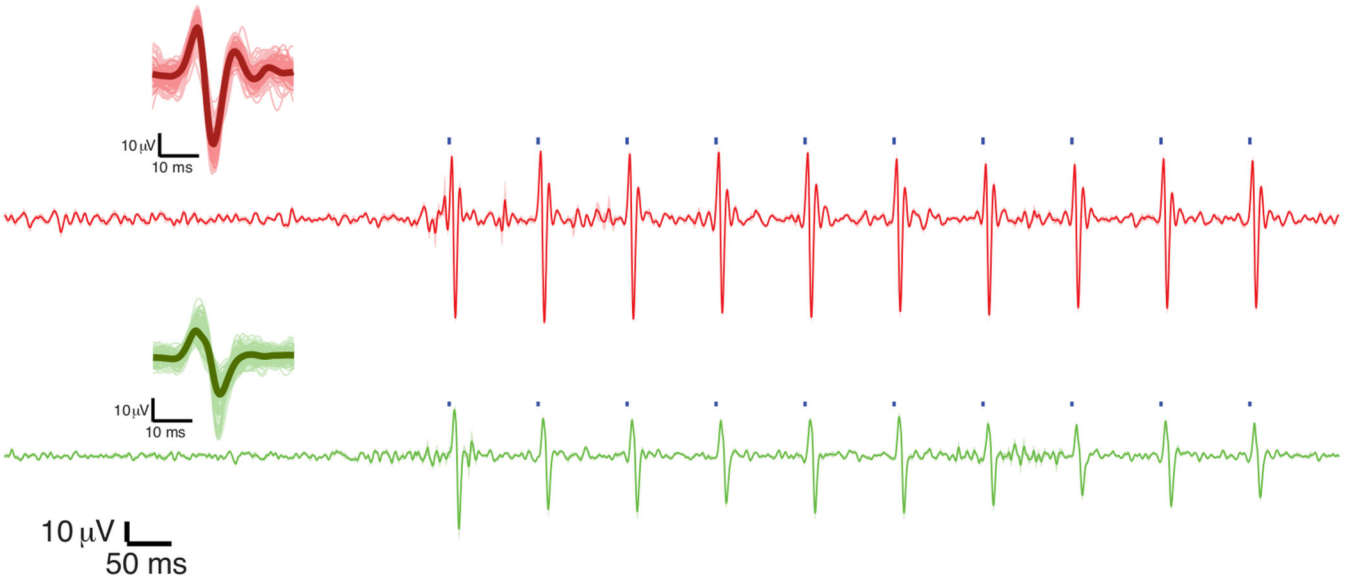

Figure 4.

Electrophysiological recordings of light-evoked activity. Micro-Electrocorticography (μECoG) recordings occurred during pulsed optical stimulation. Recording traces were from the closest electrode to the site of stimulation for examples of M1 (red) and S1 (green) stimulation locations. Shaded areas around the traces represent standard error across 25 trials. The blue squares on the traces show the timing of stimulation (1 ms). The full set of stimulus-triggered waveforms for both sample pairs of stimulation and recording sites are superimposed on the mean waveform as shown on the left side of the panel. This figure has been modified from Yazdan-Shahmorad *et al.* 2016[9].

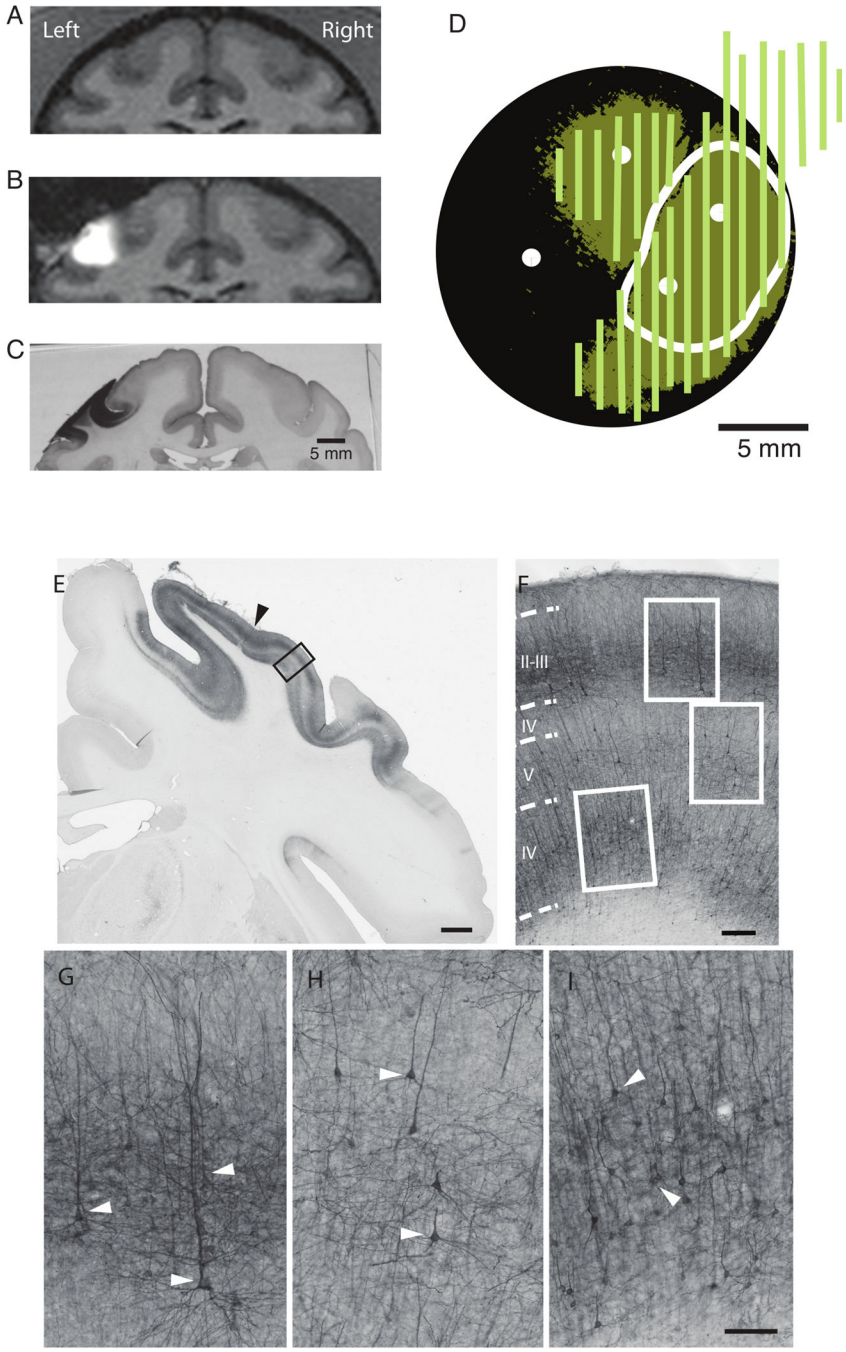

Figure 5.

Histological analysis. A) Baseline coronal MR image in monkey G. B) Spread of contrast agent after the infusion for the same MR coronal slice as in A. C) A coronal tissue section from approximately the same site as in A and B; peroxidase staining reflects expression of the EYFP-reporter. D) Good alignment is observed between the area of EYFP expression measured with surface epiflourescence (dark green areas) and with histological staining (light green lines). These include the region of vector spread estimated from MR images (white line); white dots indicate injection sites, and the entire black region represents the

area exposed by the craniotomy. The two left most injection sites are located in M1, and the two right most sites are located in S1. E) Low magnification image of the coronal section stained with anti-GFP antibody showing the medio-lateral aspect of YFP expression in the somatosensory cortex of monkey J (areas 1, 2, 3). The black arrowhead indicates the location of the cannula track; the adjacent tissue (black frame) is shown in F, at greater magnification to show laminar distribution of the YFP-positive cells. F) Densely populated regions of YFP-positive cells are located predominantly in layers II-III and V-VI, and also show typical pyramidal morphology (cells in white frames are further enlarged in panels G-I). White arrowheads on bottom panels G-I point to typical pyramidal cells in layers II-III (G); layer V (H); and layer VI (I). Scale bars: A, 2 mm; B, 200 μm; C-E, 100 μm. This figure has been modified from Yazdan-Shahmorad *et al.* 2016[9] and Yazdan-Shahmorad *et al.* 2018[15].

Table of materials

Name of Material/ Equipment	Company	Catalog Number	Comments/Description
0.2 mL High Pressure IV Tubing	Smiths Medical Inc., Dublin, OH, USA	533640	
0.32 mm ID, 0.43 mm OD Silica Tubing	Polymicro Technologies	1068150027	
0.45 mm ID, 0.76 mm OD Silica Tubing	Polymicro Technologies	1068150625	
AAV2.5-CamKII-C1V1-EYFP	Penn Vector Core, University of Pennsylvania		
ABS plastic	Stratasys, MN, USA	ABS*plus*-P430	
Antimicrobial incise drape	3M	6650EZ	Ioban Drape
Dental Acrylic	Henry Schein, Inc.	1013117	Acrylic Bonding Agent
Elevators	VWR International, LLC.	10196-564	Langenbeck Elevator, Wide Tip
Fine suture	McKesson Medical-Surgical Inc.	1034505	
Gadoteridol	Prohance, Bracco Diagnostics, Princeton, NJ	0270-1111-04	
Laser for light stimulation	Omicron-Laserage, Germany	PhoxX 488-60	
MR compatible 3cc syringe	Harvard apparatus, Holliston, MA, USA	59-8377	
MR Imaging Software	Pixmeo	OsiriX MD 10.0	
MR-Compatible Pump	Harvard apparatus, Holliston, MA, USA	Harvard PHD 2000	
MR-compatible stereotaxic frame	KOPF	1430M MRI	
Perifix Clamp Style Catheter Connector	B-Braun, Bethlehem, PA, USA	N/A	
Plastic Screws	Plastics 1	0–80 × 1/8N	Nylon screws
Titanium screws	Crist Instrument Co., Inc.	6-YCX-0312	Self-tapping bone screws
Trephine	GerMedUSA Inc,	SKU:GV70-42	
uPrinter SE 3D printer	Stratasys, MN, USA	N/A	
Vitamin E Capsule	Pure Encapsulations, LLC.	DE1	
Wet sterile absorbable gelatin	Pfizer Inc.	AZL0009034201	Gelfoam